RSC Advances

PAPER

View Article Online
View Journal | View Issue

Cite this: *RSC Adv.*, 2023, **13**, 24617

A reliable QSPR model for predicting drug release rate from metal–organic frameworks: a simple and robust drug delivery approach†

Leila Tayebi, Rahmatollah Rahimi, Ali Reza Akbarzadeh * and Ali Maleki

During the drug release process, the drug is transferred from the starting point in the drug delivery system to the surface, and then to the release medium. Metal–organic frameworks (MOFs) potentially have unique features to be utilized as promising carriers for drug delivery, due to their suitable pore size, high surface area, and structural flexibility. The loading and release of various therapeutic drugs through the MOFs are effectively accomplished due to their tunable inorganic clusters and organic ligands. Since the drug release rate percentage (RES%) is a significant concern, a quantitative structure–property relationship (QSPR) method was applied to achieve an accurate model predicting the drug release rate from MOFs. Structure-based descriptors, including the number of nitrogen and oxygen atoms, along with two other adjusted descriptors, were applied for obtaining the best multilinear regression (BMLR) model. Drug release rates from 67 MOFs were applied to provide a precise model. The coefficients of determination (R^2) for the training and test sets obtained were both 0.9999. The root mean square error for prediction (RMSEP) of the RES% values for the training and test sets were 0.006 and 0.005, respectively. To examine the precision of the model, external validation was performed through a set of new observations, which demonstrated that the model works to a satisfactory degree.

Received 4th January 2023
Accepted 5th June 2023

DOI: 10.1039/d3ra00070b

rsc.li/rsc-advances

1. Introduction

Cancer is one of the major diseases affecting human health, and morbidity has increased gradually.[1] Although the remedies for cancer have progressed and survival rates have increased in recent years, the heterogeneity of cancer necessitates further effective treatment strategies.[2] Cancer involves uncontrolled cell division and tissue invasion (metastasis) caused by a series of mutations in the genes of proteins that regulate the cell cycle.[3] These mutations typically involve either promotion of cell division or the inactivation of cell cycle suppression.[4] With our changing daily lifestyle and social environment, non-communicable diseases have become the leading cause of death.[5] Cancer is caused by significant changes in and damage to genes,[6] which may be accidental or *via* exposure to carcinogens. A carcinogen includes chemical substances, such as arsenic and asbestos,[7,8] or environmental, viral, or genetic factors.[9] Cancer risk factors are classified into four main classes: (a) biological factors, such as age, gender, and genetic diseases; (b) carcinogen exposure, for instance, to radioactive radiation, many chemicals, and some particulate materials; and (c) lifestyle-related factors such as tobacco, alcohol, and exposure to UV radiation in sunlight.[10]

Ways to treat cancer include surgery, chemotherapy, radiation therapy, targeted therapy, immunotherapy, stem cell or bone marrow transplant, and hormone therapy.[11] Generally, cancer drugs destroy the RNA or DNA responsible for replication in cell division; therefore, the cancer cells are unable to divide and die.[12] Chemotherapy drugs kill cancer cells by stopping them from growing and multiplying.[13] If the cells can't grow and multiply, they usually die. Some chemotherapy drugs target a specific stage of the cell cycle.[14] The fluoropyrimidine 5-fluorouracil (5-FU) is an effective antimetabolite drug that is widely used for the treatment of cancer, especially colorectal cancer. The action of 5-FU is through the inhibition of thymidylate synthase (TS) and incorporation of its metabolites into RNA and DNA.[15]

Unfortunately, chemotherapeutic drugs in free formation always lead to adverse effects on healthy tissues and even the immune system. Nanocarriers have been intensively engineered as stimuli-responsive drug delivery systems to load and intelligently release various drug molecules. To achieve superior efficacy, the drugs need to be loaded into nanocarriers with high loading content and released at the target site in a controllable and specific-responsive manner.[16] Further, various nanoparticle-based systems have been studied for drug delivery, such as liposomes, micelles, dendrimers, microbubbles, and

Department of Chemistry, Iran University of Science and Technology, P. O. Box: 16846-13114, Tehran, Islamic Republic of Iran. E-mail: a_akbarzadeh@iust.ac.ir

† Electronic supplementary information (ESI) available. See DOI: https://doi.org/10.1039/d3ra00070b

solid particles.[17] Due to their suitable pore size and diverse functional groups, as well as great loading of drugs, metal–organic frameworks (MOFs) are potentially beneficial to encapsulate drug products.[18] Furthermore, MOFs show several outstanding advantages, such as facile modification of physical and chemical properties through inorganic clusters and/or organic ligands.[19]

The quantitative structure–activity relationship (QSAR) model is a regression model in which the relationship between chemical structure and biological action is quantitatively investigated.[20] The basis of QSAR methods is the dependence on action and structure.[21] Quantitative dependence on action and structure is one of the most fundamental methods of intra-computer study for biological and chemical modeling, especially in drug design, drug targeting, and drug discovery.[22] The quantitative structure–property relationship (QSPR) method applies structural features of molecules to create an accurate and fast model that correlates structure-based properties of materials to their quantitative functions. Generally, there are two common categories for QSPR models, based on the type of descriptors used in modeling: theory- and experiment-based modeling. To build a theory-based QSPR model, various molecular descriptors, such as geometric, quantum mechanical, and thermodynamic quantities are used, and experiment-based QSPR models are mainly presented using experimental descriptors that express the physicochemical properties related to the structure of molecules.[23] QSPR investigations on drug release from hydroxypropyl methylcellulose compounds have been conducted using structural descriptors; these have confirmed that the aqueous solubility of drugs and the size of the drug molecules are appropriate descriptors that can influence drug release from these polymers.[24] Also, penetration enhancement activities of some compounds towards different drugs have been investigated, employing a QSPR study.[25] This QSPR technique was developed using the molecular descriptors created by the COSMIC force field and the molecular mechanical descriptors by the NEMESIS software; which helps to better understand the mechanisms of penetration enhancement.[25] A prediction of the volume of distribution has been created by Ghafourian *et al.* using some structural descriptors, including partitioning, quantum mechanical, molecular mechanical, and connectivity parameters.[26] Selection of the proper variable was made using a genetic algorithm, and stepwise regression analyses and many models were created for acidic and basic drugs. Furthermore, QSPR analysis of many MOFs has been developed by researchers to correlate their structural features and their physical, chemical, and biological properties.[27–29] To develop a QSPR/QSAR model, several mathematical methods have been applied. Multiple linear regression (MLR), partial least squares (PLS), principal component analysis (PCA), and artificial neural network (ANN) are four commonly used methods.[23]

In this research, based on structural variables—such as ligand fragments and metal secondary building units (SBUs)—as the adjusted parameters, we obtained the most appropriate drug release model from MOFs through the QSPR method, which was performed using 5-FU drug release. The presented procedure here investigated the relationships between the release of drugs from a large class of MOFs and their structures. This work indicates a simple computational method for the rapid calculation of drug release from MOF drug delivery systems with suitable results. Considering that 5-FU is widely used for cancer treatment, the model was specifically created for this drug. One of the challenges we face in modeling drug release from drug delivery systems is that the desired software is not available to everyone. In addition, the determination of quantum descriptors is a complex process. The advantage of the presented work is that (a) the model is performed without special software, and (b) modeling is carried out using simple and knowledge-based descriptors.

2. Materials and methods

The studied dataset of MOFs containing different metal SBUs and various organic linkers, as drug delivery systems, was collected from different scientific research studies. The experimental data of the drug release rate of different MOFs were gathered and tested for the delivery of 5-fluorouracil (5-FU) in several cancer cell lines. Drug delivery data for 5-FU were collected because 5-FU has a small size and is widely used as an anticancer chemotherapy drug for the treatment of several cancers. The measured drug release rate is expressed as a percentage (RES%). The RES% for 67 metal–organic frameworks were collected from the literature. Table 1 lists the MOFs together with the experimental RES% for 5-FU collected from the literature. The best multilinear regression (BMLR) model was created using a set of 54 MOFs as a training set (80% of all data), which was then applied to 13 MOFs as a test set (20% of all data) to evaluate the predictive ability of the model. External validation is a validation strategy to ensure that the BMLR model is accurate for the prediction of dependent variables, using external data that was not used to develop the model. After the regression model has been obtained from the original dataset, the new data points investigate the model's validity. Hereupon, eight observations were used to form the external test set. The molecular structures of organic linkers for the training and test sets are illustrated in Table S1 (ESI).†

The statistical coefficients, R^2 (coefficient of determination) and $R_{adj}{}^2$ (the adjusted R-squared), were calculated as follows (eqn (1) and (2)):

$$R^2 = 1 - \frac{\sum (y_i - \hat{y}_i)^2}{\sum (y_i - \bar{y})^2} \quad (1)$$

$$R_{adj}{}^2 = 1 - \left[\frac{(1 - R^2)(n-1)}{n-k-1}\right] \quad (2)$$

where y_i, $\bar{y}$ and $\hat{y}_i$ are the observed, average, and calculated values of the dependent variable, respectively. The value n is the number of points in the data sample, and k is the number of independent regressors. The formula for Q^2 is the same, but the difference is that calculated values have been replaced by the predicted values (eqn (3)):

$$Q^2 = 1 - \frac{\sum (y_{iTR} - \hat{y}_{iTR})^2}{\sum (y_i - \bar{y})^2} \quad (3)$$

Table 1 Experimental and theoretical values of drug release rate from MOFs for training (no. 1–54), test (no. 55–67), and validation test sets (no. 68–75)

No.	MOF	n_N	n_O	RES$^+$	RES$^-$	Exp. RES%[a]	I_{M-L}	Ref.	Pred. RES%[b]	Dev.[c]	Std. dev.[d]	L.B. 95%[e]	U.B. 95%[f]
Training set (54 entries)													
1	NTU-Z11	0.00	16.00	1.377	2.550	64.00	−5.91	32	28.991	0.009	−0.026	63.991	64.009
2	CPON-1	1.00	5.00	−0.220	2.811	25.00	−3.27	33	23.994	0.006	0.556	24.989	25.006
3	$[(CH_3)_2NH_2]_2[Zn(TATAT)_{2/3}]\cdot 3DMF$	9.00	12.00	−7.698	4.739	44.00	−9.95	34	51.994	0.006	1.055	43.987	44.004
4	fa-IRMOF3	3.00	13.00	−2.189	3.300	45.00	−5.09	35	14.999	0.001	2.116	44.983	45.000
5	$[(Me_2NH_2)_4Zn_2(FDC)_4]_n$	4.00	20.00	−5.491	3.664	29.00	−7.70	36	25.993	0.007	−1.934	29.000	29.017
6	$[Zn_3(BTC)_2(Me)(H_2O)_2](MeOH)_{13}$	0.00	33.00	−4.982	2.627	18.00	−9.95	37	31.003	−0.003	0.149	17.991	18.008
7	$[Zn_3(bdcNH_2)_2(dfp)_2]\cdot DMF$	4.00	12.00	0.227	3.712	89.00	−13.05	38	51.999	0.001	−1.332	88.997	89.015
8	$NH_2(CH_3)_2[Zn_3(L)_2\cdot 3.5DMF]$	0.00	16.00	−0.596	4.440	22.00	−9.60	39	42.999	0.001	1.293	21.986	22.003
9	IRMC-1	12.00	1.00	−5.553	5.521	85.00	−7.27	40	11.993	0.007	−0.200	84.991	85.010
10	$[Zn_2(ad)_2(hmdb)(H_2O)](DMF)_2$	15.00	12.00	−17.118	2.995	13.00	−19.86	41	19.992	0.008	−0.216	12.992	13.010
11	$[Zn(FDC)]\cdot H_2O$	0.00	5.00	1.375	2.624	34.00	−1.09	42	51.999	0.001	−1.981	34.000	34.017
12	$[Zn(BTC)(HME)]\cdot(DMAc)(H_2O)$	7.00	8.00	−6.494	3.260	31.00	−8.48	43	22.996	0.004	1.757	30.984	31.001
13	$[Zn_2(ad)_2(fmdb)(H_2O)](DMF)_3$	10.00	15.00	−11.880	4.244	11.00	−14.79	44	23.991	0.009	−0.969	10.995	11.013
14	$[Zn_3(OH)_2(H_2tccp)_2(bpy)_2](H_2O)_3(DMF)_3$	6.00	18.00	−6.142	5.810	29.00	−14.22	45	63.998	0.002	0.412	28.989	29.007
15	$[Zn_8(O)_2(CDDB)_6(DMF)_4(H_2O)]$	10.00	31.00	−13.260	3.020	43.00	−17.87	46	45.991	0.009	−2.038	43.000	43.017
16	$[Zn_2(ad)_2(AMDB)(H_2O)](DMF)_3$	17.00	10.00	−18.100	3.533	20.00	−20.87	47	47.995	0.005	0.245	19.990	20.008
17	$[Zn_2(bptc)(H_2O)]\cdot(DMAc)_3(H_2O)_4$	3.00	16.00	−4.027	3.400	26.00	−7.02	48	9.998	0.002	−0.741	25.995	26.012
18	$[Zn(4,4\text{-bipy})(formic\ acid)_2(NO_3)_2]$	1.00	4.00	−0.836	2.334	17.00	−8.83	49	56.199	0.001	0.266	16.990	17.008
19	$([Zn_4O(dmcapz)_3]$	6.00	7.00	−2.396	5.965	52.00	−5.40	50	39.991	0.009	0.540	51.989	52.007
20	$[Zn_7L_2(HL)_2(OH-)_4(H_2O)_2]\cdot 2H_2O$	4.00	40.00	−10.174	3.465	17.00	−12.62	51	83.997	0.003	−0.433	16.993	17.011
21	$[Zn_2(fer)_2]$	0.00	8.00	0.449	1.088	40.00	−8.23	52	95.001	−0.001	−0.697	39.994	40.012
22	$[Zn_2(abtc)(DMA)(H_2O)_2]\cdot(DMA)_4$	3.00	11.00	−1.637	4.194	41.00	−9.12	53	78.991	0.009	−0.070	40.992	41.009
23	$[(Me_2NH_2)_2Zn_3(fdc)_4]_n\cdot DMA$	2.00	20.00	−0.153	3.664	75.00	−5.35	54	28.991	0.009	−0.378	74.993	75.010
24	ZIF-NP	5.00	4.00	−2.293	1.896	60.00	−4.65	55	23.994	0.006	0.907	59.987	60.005
25	ZIF-90	2.00	0.00	0.552	2.375	41.00	−7.57	56	51.994	0.006	−0.218	40.992	41.010
26	Cu-BTC	0.00	12.00	1.356	2.550	53.00	−13.30	57	14.999	0.001	−0.151	52.992	53.009
27	$[Cu(L)(4,4'\text{-bipy})(H_2O)]_n\cdot 1.5nCH_3CN$	3.50	5.00	−3.353	3.235	15.00	−26.65	58	25.993	0.007	−1.176	14.996	15.014
28	$[(Cu_2(L_2)(H_2O)_2]\cdot 2.22DMA$	3.22	12.20	−3.335	4.095	24.00	−19.77	59	31.003	−0.003	0.473	23.989	24.007
29	GDMU-2	0.00	14.00	−0.794	5.100	9.00	−20.12	60	51.999	0.001	1.042	8.987	9.004
30	$[Cu(BTTA)]_n$	6.00	4.00	−4.745	5.334	15.00	−6.93	61	42.999	0.001	0.446	14.989	15.007
31	$[NH_2(CH_3)][Cu_6(L)_3(OAc)(H_2O)_4]\cdot x$solvent	10.00	30.00	−13.703	5.211	18.00	−28.52	62	11.993	0.007	−0.953	17.995	18.013
32	$[H_3O][Cu_6(tpta)_3(DMA)_4(COO)]\cdot 12H_2O\cdot 7DMA$	4.00	30.00	−7.078	3.400	35.00	−26.73	63	19.992	0.008	1.097	34.987	35.004
33	$[Cu_2(OH)bcb](DMF)_2(H_2O)_3$	0.00	9.00	0.993	4.028	29.00	−20.22	64	51.999	0.001	1.010	28.987	29.004
34	$[Dy(BTC)(H_2O)]\cdot(H_2O)(DMF)$	0.00	6.00	0.450	2.550	24.00	−9.85	65	22.996	0.004	0.174	23.991	24.008
35	$[Dy(HABA)(ABA)](DMA)_4]$	27.00	6.00	−26.397	2.198	52.00	−67.28	66	23.991	0.009	0.657	51.987	52.007
36	$[Gd(BCB)(DMF)](H_2O)_2$	1.00	10.00	−1.050	4.386	15.00	−47.01	67	63.998	0.002	−1.063	14.996	15.013
37	$[Gd_2(H_2O)_3(SDBA)_3](DMA)_3]$	3.00	15.00	−3.987	3.114	26.00	−48.84	68	45.991	0.009	0.422	25.990	26.007
38	$[In(Hpbic)(pbic)](DMF)_2$	6.00	4.00	−4.715	3.200	31.00	−15.35	69	47.995	0.005	−1.747	30.999	31.016
39	$[Co(SDB)(bpdh)_{0.5}]_n$	2.00	6.00	2.064	6.027	52.00	−19.06	70	9.998	0.002	−0.637	51.994	52.012
40	$[Ca_3(TATAB)_2(H_2O)(MeOH)](DMF)_3$	12.00	14.00	−12.910	1.630	43.00	−18.70	71	56.199	0.001	−0.814	42.995	43.012
41	$Mg(H_2TBAPy)(H_2O)_3\cdot C_4H_8O_2$	0.00	13.00	−1.265	3.400	12.00	−9.40	72	39.991	0.009	0.258	11.990	12.008
42	$[Co_2(L)(4,4'\text{-Bipy})_2]\cdot CH_3CN$	6.00	10.00	−5.475	5.418	20.00	−13.87	73	83.997	0.003	0.620	19.989	20.006
43	$[Sr(HTATB)(H_2O)_2](DMF)_4$	3.00	7.00	−0.290	3.860	52.00	−9.77	74	95.001	−0.001	−0.585	51.994	52.011
44	$[Ba(HTATB)(H_2O)_2](DMF)_4$	7.00	12.00	−7.495	3.860	23.00	−15.84	75	78.991	0.009	−0.162	22.992	23.009
45	MIL-100 (Fe)	0.00	24.00	−2.918	2.550	24.00	−7.88	76	28.991	0.009	0.988	23.987	24.005
46	UiO-66	0.00	20.00	0.195	1.700	64.00	−7.78	77	23.994	0.006	−0.289	63.992	64.010
47	MIL-101-NH_2-Fe	4.00	16.00	−4.873	1.082	46.00	−10.54	78	51.994	0.006	1.168	45.986	46.004
48	MIL-88B	0.00	24.00	−0.211	4.564	48.00	−7.44	79	14.999	0.001	0.237	47.990	48.008
49	UiO-66-COOH	1.00	4.00	−1.025	2.922	10.00	−6.36	80	25.993	0.007	−0.932	9.995	10.013
50	CP5-capped UiO-66-NH-Q	7.00	62.00	−14.774	3.377	56.20	−20.31	81	31.003	−0.003	−0.442	56.192	56.212
51	MOF-In1	0.00	20.00	−0.646	3.342	40.00	−8.55	82	51.999	0.001	1.074	39.987	40.004
52	Mn-ZIF-90	4.00	2.00	1.068	2.380	84.00	−2.09	83	42.999	0.001	0.036	83.991	84.009
53	UiO-67-$(NH_2)_2$	12.00	32.00	−13.236	0.464	95.00	−20.00	84	11.993	0.007	−0.570	94.993	95.012
54	DCA-UiO-DTDP-FA	14.00	36.00	−17.144	0.622	79.00	−22.83	85	19.992	0.008	1.759	78.983	79.002
RMSEP		0.006											
Test set (13 entries)													
55	$[Zn_3(\mu_3\text{-}O)(BTC)_2(DMF)]\cdot 2NH_2(CH_3)_2\cdot 4H_2O$	3.00	18.00	−3.087	2.550	51.00	−10.32	32	50.999	0.001	−0.559	50.993	51.011
56	$[Zn(bptc)(H_2O)]\cdot(DMA)_4$	4.00	13.00	−4.317	3.400	29.00	−10.09	86	28.991	0.009	1.206	28.986	29.005

Table 1 (*Contd.*)

No.	MOF	n_N	n_O	RES^+	RES^-	Exp. RES%[a]	I_{M-L}	Ref.	Pred. RES%[b]	Dev.[c]	Std. dev.[d]	L.B. 95%[e]	U.B. 95%[f]
57	$[Zn_2(L)(H_2O)_{1.5}]\cdot 5H_2O$	1.00	9.50	−0.476	4.095	24.00	−7.09	87	23.995	0.005	0.405	23.988	24.009
58	$[Zn_3(bdc)_2(dfp)_2]\cdot 2DMF$	2.00	12.00	0.844	4.330	63.00	−13.64	38	62.996	0.004	0.236	62.988	63.010
59	$[Zn(H_2O)_6K_2(H_2BTC)_2(H_2O)_4](H_2BTC)_2\cdot 2H_2O$	0.00	36.00	−3.904	2.550	42.00	−8.06	88	41.993	0.007	0.819	41.986	42.008
60	ZIF-8	5.00	4.00	−3.831	1.896	38.00	−6.19	89	37.998	0.002	−0.325	37.991	38.011
61	$[(Zn_2(L1)(DMA)]\cdot 1.75DMA$	3.75	10.75	−3.975	4.095	19.00	−7.04	59	18.998	0.002	−0.830	18.993	19.013
62	ZIF-90	2.00	0.00	0.482	2.375	40.00	−7.64	90	39.996	0.004	0.744	39.988	40.007
63	$[Zn_{10}(OH)O(BTC)_5(HBTC)(DMA)_2(H_2O)_4]\cdot 11DMA$	13.00	55.00	−21.242	2.550	42.00	−27.15	91	41.991	0.009	−0.330	41.989	42.013
64	$[Dy_2(L)_2(H_2O)_2]_n$	0.00	14.00	0.912	2.550	52.00	−10.18	92	51.999	0.001	−0.058	51.991	52.010
65	FA-MOF-808	0.00	12.00	0.797	2.550	45.00	−5.48	93	45.005	−0.005	−1.695	44.997	45.016
66	FA-NH_2-UiO-66	4.00	20.00	−5.901	1.082	42.00	−13.01	93	41.994	0.006	0.877	41.987	42.007
67	MIL-88B	0.00	20.00	−2.743	1.700	22.00	−38.24	94	21.999	0.001	−0.492	21.991	22.012
RMSEP		0.0052											
External validation test set (8 entries)													
68	$Zn_6(L)_3(DMA)_4]\cdot 5DMA$	9.00	33.00	−10.35	3.400	72.00	−13.61	95	71.998	0.002	−0.931	71.986	72.022
69	$[Zn_3(BTC)_2(Aml)(H_2O)_2](MeOH)_6$	6.00	14.00	−7.12	2.296	30.00	−12.12	96	29.997	0.003	−0.519	29.985	30.019
70	$[[Dy_2(H_2O)_3(SDBA)_3](DMA)_6]$	0.00	21.00	−1.72	3.114	29.00	−12.00	97	28.990	0.010	0.551	28.980	29.015
71	$[Gd_2(TATAB)_2]\cdot 6DMF$	12.00	12.00	−11.28	1.630	61.00	−49.29	98	60.997	0.003	0.090	60.982	61.017
72	$[Mg_3(H_2O)_4(5\text{-aip})_2(5\text{-Haip})_2]\cdot 4DMA$	8.00	24.00	−9.00	1.082	69.00	−13.89	99	68.991	0.009	0.869	68.979	69.014
73	$[Ca_3(TATB)_2(H_2O)](DMF)_4(H_2O)$	6.00	13.00	−2.78	3.860	78.00	−12.06	100	77.994	0.006	0.671	77.979	78.015
74	NanoHKUST-1	0.00	12.00	2.06	2.550	63.00	−3.65	101	62.996	0.004	−0.167	62.985	63.017
75	Fe-MIL-53-NH_2	1.00	4.00	2.37	1.082	72.00	−3.70	102	71.999	0.001	−0.565	71.985	72.020
RMSEP		0.0054											

[a] Exp. RES%: experimental value of RES%. [b] Pred. RES%: predicted value of RES%. [c] Dev.: deviation. [d] Std. dev.: standard deviation. [e] L.B.: lower bound. [f] U.B.: upper bound.

where y_{iTR} and $\hat{y}_{iTR}$ show the observed and calculated values for the training set, respectively. Other statistical parameters, including ${Q_{F1}}^2$, ${Q_{F2}}^2$, and ${Q_{F3}}^2$ are calculated using eqn (4)–(6):

$$ {Q_{F1}}^2 = 1 - \frac{\sum (y_i - \hat{y}_i)^2}{\sum (y_i - \overline{y}_{tr})^2}, \quad (4) $$

$$ {Q_{F2}}^2 = 1 - \frac{\sum (y_i - \hat{y}_i)^2}{\sum (y_i - \overline{y}_{test})^2} \quad (5) $$

$$ {Q_{F3}}^2 = 1 - \frac{\sum (y_i - \hat{y}_i)^2 / n_{test}}{\sum (y_i - \overline{y}_{tr})^2 / n_{tr}} \quad (6) $$

where $\bar{y}_{test}$ indicates the average values for the test set. The model accuracy is defined by the concordance correlation coefficient (CCC), which is calculated by eqn (7) as follows:

$$ {Q_{CCC}}^2 = \frac{\sum (y_i - \overline{y})\left(\hat{y}_i - \overline{\hat{y}}\right)}{\sum (y_i - \overline{y})^2 + \sum \left(\hat{y}_i - \overline{\hat{y}}\right)^2 + \sum \left(\overline{y} - \overline{\hat{y}}\right)^2} \quad (7) $$

After the BMLR model has been developed with the original dataset, the new observations (the new set of compounds) investigate the model's validity by computing ${Q_{(Ext)}}^2$, ${Q_{(Ext)F1}}^2$, ${Q_{(Ext)F2}}^2$, ${Q_{(Ext)F3}}^2$, and ${Q_{(Ext)CCC}}^2$.

3. Results and discussion

A reliable correlation for the prediction of drug release rate from MOFs containing different metal SBUs and various organic linkers was obtained in this research. The QSPR modeling for the abovementioned dataset was performed using SPSS software (version: 1.0.0.1406). The number of nitrogen and oxygen atoms, as well as the two adjustable parameters, comprise four variables employed to build the correlation by multiple linear regression model (eqn (8)). These descriptors were created based on our knowledge of chemistry, without using the software. The mentioned descriptors are knowledge-based and obtained through advanced inorganic chemistry theories with tedious work. The descriptors were selected in such a way that, on the one hand, they are related to the chemical structure of the MOF, and on the other hand, they can have a reasonable impact on the drug release rate (RES%). Several descriptors were examined for this purpose, and finally, these four descriptors were selected, which created the maximum R^2 and minimum RMSE; also, they do not have a high correlation coefficient with each other.

$$ \begin{aligned} RES\% = {} & 20.135 + 15.157 n_N + 2.675 n_O \\ & - 7.300 RES^- + 14.296 RES^+ \end{aligned} \quad (8) $$

where RES% represents the values of drug release rate in percentage from the MOFs; n_N is the number of nitrogen atoms;

Table 2 RES^{-} values specified for molecular fragments of linkers

Class	Effective fragments	Substituents			RES^{-}
Aryl compound	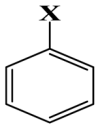	X:	–COOH		0.850
			$-NO_2$		0.915
			–OH		−0.900
			$-NH_2$		−0.618
			–NH–C		−0.460
			–NH–Ar		−0.352
			–CO–NH		0.680
			–C–Ar		0.145
			–O–C		0.314
			$-SO_2-Ar$		1.414
			–CO–Ar		0.612
			–P=O		0.264
			–N=N–Ar		0.794
Aromatic	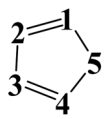	5 = O & 1,2,3,4 = C			0.720
		5 = N & 1,2,3,4 = C			1.320
		1,4 = N & 2,3,5 = C			1.645
		1,5 = N & 2,3,4 = C			1.655
		1,4,5 = N & 2,3 = C			1.801
		1,2,4 = N & 3,5 = C			1.811
		1,3,5 = N & 2,4 = C			1.817
		1,2,3,5 = N & 4 = C			1.860
	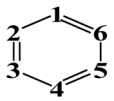	1 = N & 2,3,4,5,6 = C			0.695
		1,3 = N & 2,4,5,6 = C			1.010
		1,6 = N & 2,3,4,5 = C			1.020
		1,3,5 = N & 2,4,6 = C			1.310
Aliphatic	C_nH_{2n}	$n = 2$			0.186
	C_nH_{2n+1}	$n = 1$			0.251
N-functional		–C–NH_2			−0.411
		–C=N–N=C–			1.021
					1.780
		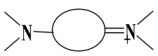			1.840
O-functional		R–(CO)OH	R:	H	0.944
				C	0.952
		R–(CO)–R		H	0.730
				C	0.700
		C–OR		H	−0.742
					2.014
Halide		X: F			0.330
		$[NH_2(CH_3)_2]^+$			1.040
Ion fragments	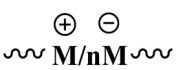				1.560

n_O is the number of oxygen atoms of the desired MOF. RES^{+} and RES^{-} are two new descriptors that increase and decrease the RES%; they exhibit the contribution of d-orbitals of metal SBUs and molecular fragments of linkers, which affect the RES% from MOFs, respectively. According to the resulting model, the increaser values are well defined, and it was found that not only the impact of metal should be considered to determine the RES^{+} values, but also the ligand effects are significant; therefore, the effect of ligand interaction with the metal center was evaluated, and RES^{+} was calculated. To create an MLR model, a suitable database containing 67 metal–organic frameworks was studied, and the experimental data for drug release rates from these MOFs are given in Table 1.

According to our previous works,[30,31] to estimate the important properties of materials, simple group-contribution methods can be employed, and the values of RES^{-} were determined based on this technique. This study found a reliable contribution between various particular molecular fragments of

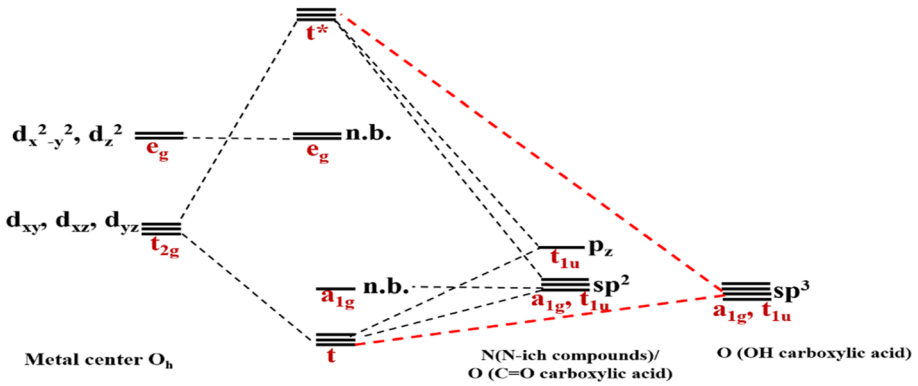

Fig. 1 Molecular orbital diagram indicating the interaction of metal d-orbitals and the heteroatoms of linkers.

the linker and the drug release rate from MOFs, RES%. Table 2 lists different RES^- values; these values have been determined for several molecular fragments of linkers, which are the result of the core correlation. In Table 2, for the substituents containing nitrogen or oxygen attached to one or more rings, the ring symbol is used for simplicity.

As mentioned above, RES^+ represents one of the descriptors that increase the RES%. It is obtained from eqn (9) and consists of two parts: RES_M and I_{M-L}. The RES_M results from eqn (10) and is calculated by considering the molecular weight of MOF and the atomic mass of oxygen and nitrogen, as well as the impact of d-orbitals of the metal center. I_{M-L} describes the interaction between the d-orbitals of the metal center and the valence orbitals of heteroatoms of linkers. The I_{M-L} value resulted from our experimental inorganic chemistry knowledge and can be applied to a variety of interactions. Fig. 1 represents the molecular orbital diagram resulting from the interaction of metal d-orbitals and the heteroatoms of linkers for an octahedral geometry of SBU, as an example.

$$RES^+ = RES_M + I_{M-L} \quad (9)$$

$$RES_M = [(MOF_{M_w})/(n_O m_O + n_N m_N)] \times \sum Ed_{(SBU)} \quad (10)$$

where MOF_{M_w} is the molecular weight of MOF; m_O and m_N are the atomic mass of oxygen and nitrogen, respectively. $\sum Ed_{(SBU)}$ is defined as the total energy of d-orbitals of the metal SBU, considering its geometry.

The energies of the d-orbitals for the metal center are considered through the Krishnamurthy and Schaap findings.[103] Hence, the relative energies of d orbitals in crystal fields of different metal center geometries were calculated based on Krishnamurthy and Schaap's approach (Table 3).

In other words, first, RES_M is calculated by considering the total energies of d-orbitals of metal SBUs using Krishnamurthy and Schaap's approach, then the corresponding interaction between metal and linker heteroatom (I_{M-L} value) is added to the result in the RES^+. The values of RES^+ and I_{M-L} for the training and test sets are listed in Table 1.

In this work, the geometries of the metal centers (SBUs) of MOFs were diverse, including octahedral, trigonal bipyramid, tetrahedral, square planar, square pyramidal, pentagonal bipyramid, square antiprism, and triangular dodecahedral. If the metal center is six-coordinated in octahedral coordination geometry, the d orbitals split into two sets, as shown in Table 4, first row. According to Table 3, the field for ML_6 will be ML_6 (O_h) $= 2ML_{2(XY)} + 2ML_{(Z)}$, and the total energies of the d-orbitals for octahedral geometry are obtained as $\sum Ed_{(O_h)} = 2$ Dq. The d-orbitals of the metal center under a tetrahedral crystal field are split in e and t_2 orbitals (d_{z^2}, $d_{x^2-y^2}$) (d_{xy}, d_{xz}, d_{yz}). Regarding Table 3, the summation of d-orbital energies for tetrahedral geometry is $\sum Ed_{(T_d)} = -0.89$ Dq (Table 4, first row). Whenever the metal SBU is connected to five adjacent ligands to afford the square pyramidal environment, it causes the d orbitals to split into four groups with different energies, as listed in Table 4, second row. Considering Table 3, a square pyramidal field with C_{4V} symmetry is considered as ML_5 (C_{4V}) $= 2ML_{2(XY)} + ML_{(Z)}$, then the sum of d-orbital energies for square pyramidal configuration is derived by $\sum Ed_{(C_{4v})} = 4.57$ Dq. The square planar geometry of metal centers with D_{4h} symmetry creates a d-orbital splitting, shown in Table 4, second row. Its corresponding field is twice that of the $ML_{2(XY)}$ field, $ML_{4(S.P.)} = 2ML_{2(XY)}$, and the sum of d-orbital energies is equal to 5.14 Dq. The metal d-orbital splitting diagram for trigonal bipyramidal metal SBU geometry is illustrated in Table 4, third row. For

Table 3 Relative d-orbital energies for three primary geometric configurations

Coordination number	Metal center configuration	Relative energy of d-orbitals in units of Dq				
		d_{z^2}	$d_{x^2-y^2}$	d_{xy}	d_{xz}	d_{yz}
1	ML (*z*)	5.14	−3.14	−3.14	0.57	0.57
2	ML_2 (*XY*)	−2.41	6.14	1.14	−2.57	−2.57
4	ML_4 (T_d)	−2.67	−2.67	1.78	1.78	1.78

Table 4 Total d-orbital energies for different metal center geometries

d-orbital splitting diagram	Geo[a]	∑Ed[b]
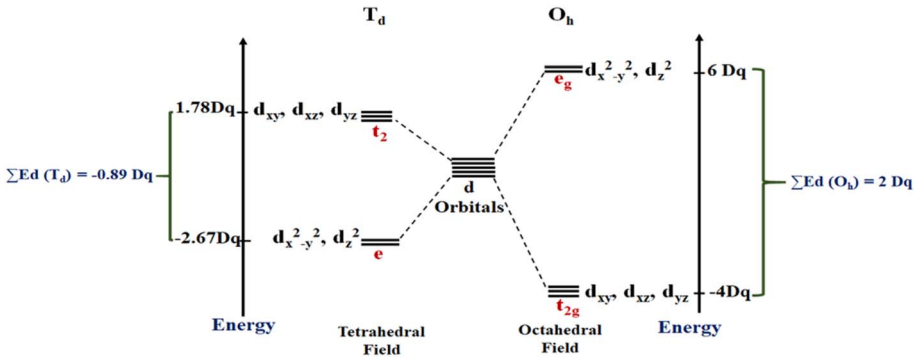	T_d	−0.890
	O_h	2.000
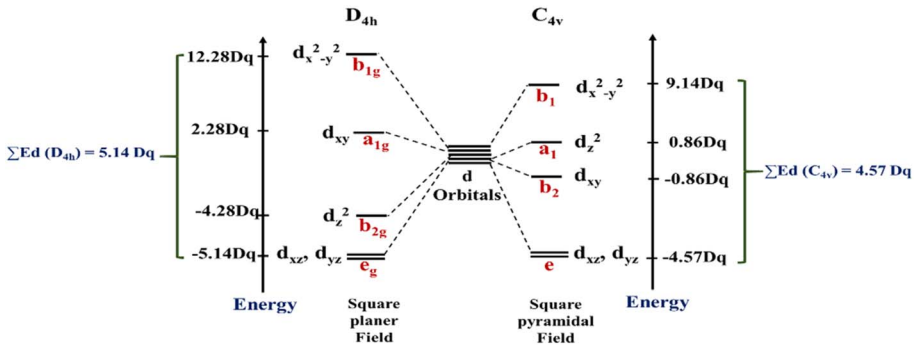	S.Py.	4.570
	S.P.	5.140
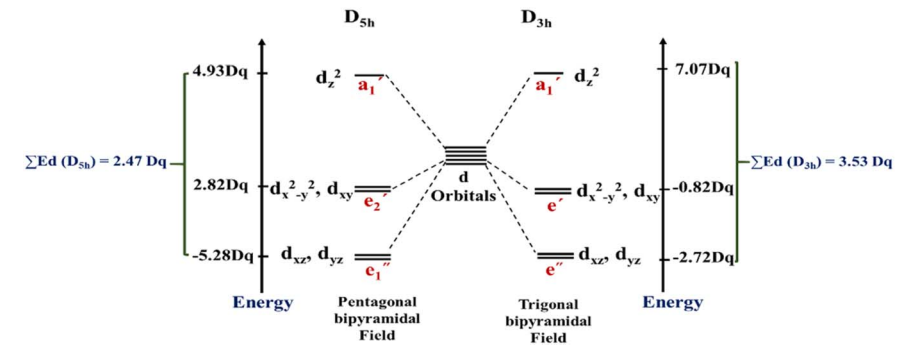	T.B.P.	3.530
	P.B.P.	2.470
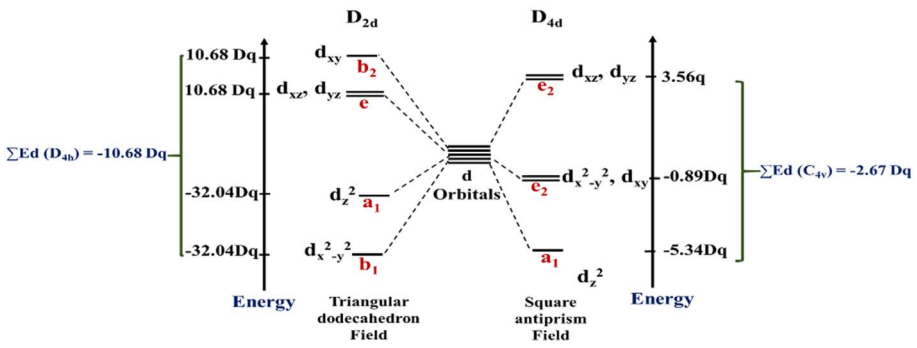	S.An.	−2.670
	T.A.D.	−10.680

[a] Geo: metal center geometry. [b] ∑Ed: total energy of d-orbitals (Dq).

T.B.Py. with symmetry D_{3h}, the respective field is $ML_5\ (T.B.Py.) = \frac{3}{2}ML_{2(XY)} + 2ML_{(Z)}$. The total energy of d-orbitals for trigonal bipyramidal geometry is $\sum Ed_{(D_{3h})} = 3.53$ Dq, and the corresponding RES^+ variables are calculated. For metal SBUs having pentagonal bipyramidal (D_{5h}), the crystal field splitting is displayed in Table 4, third row, and its field is considered as $ML_5\ (P.B.Py.) = \frac{5}{2}ML_{2(XY)} + 2ML_{(Z)}$. The consequent energies of the d orbitals is $\sum Ed = -2.47$ Dq. When the

Table 5 Correlation parameters for the validation of eqn (8) by the training, test, and external validation test sets for drug release by MOFs as drug carriers

R^2 and Q^2 tests								
Method	Sets	R^2	R_{adj}^2	Q^2	Q_{F1}^2	Q_{F2}^2	Q_{F3}^2	Q_{CCC}^2
Eqn (8)	Training set	0.9999	0.9999	—	—	—	—	—
	Test set	0.9999	0.9999	0.9999	0.9999	0.9999	0.9999	0.9999
	External validation test set	0.9999	0.9999	0.9999	0.9999	0.9999	0.9999	0.9999

Table 6 Statistical parameters of the model for the training, test, and external validation test sets

Eqn (8)	No. of MOFs	RMSEP	MSE	MAPE	F statistic	Significance F
Training set	54	0.0063	0.000	0.012	373 493 505.6	1.109×10^{-182}
Test set	13	0.0052	0.000	0.0073	35 334 456.7	5.1323×10^{-29}
External validation test set	8	0.0054	0.000	0.0044	34 571 821.9	7.988×10^{-12}

metal center is eight-coordinate, it can form square antiprism geometry with D_{4d} symmetry. The d-orbital splitting is considered in Table 4, fourth row, and concerning Table 3, its field results from $ML_8 = 2ML_4$ (T_d), but considering that in a cube, four ligands in the upper plate rotate 45°; the energy value of the d_{xy} and $d_{x^2-y^2}$ orbitals equal the average energy of the two orbitals in the cube configuration. Afterward, the resultant energies of the d orbitals are obtained by $\sum Ed_{(D_{4d})} = -2.67$ Dq. The last studied metal SBU has triangular dodecahedral geometry with D_{2d} symmetry. The metal d-orbital splitting diagram for this type of metal center geometry is exhibited in Table 4, fourth row. Its field is considered as $ML_8 = 8\frac{3}{4}ML_4$; therefore, according to Table 3, the total energy of the d orbitals is $\sum Ed = -10.68$. As mentioned above, the respective RES^+ is acquired from eqn (9), and Table 1 presents the corresponding RES^+ values.

To validate the proposed QSPR model, an external validation method was employed using new data points and the statistical parameters obtained from the model for the external set, proving the accuracy and reliability of the proposed model. From the resulting BMLR model (eqn (8)), R^2 and adjusted R^2 values both are 0.9999 for the training and test sets. As shown in Table 5, correlation parameters for the test set, including Q_{F1}^2, Q_{F2}^2, Q_{F3}^2, and Q_{CCC}^2 of the model yielded 0.9999. These correlation parameters for the external validation test set were acquired at 0.9999 as well, which demonstrated that the model is very credible and robust.

The root mean square error for prediction (RMSEP) values were 0.006, 0.0052, and 0.0054 for the training, test, and external validation test sets, respectively. Also, the mean absolute percentage errors (MAPE) were 0.012, 0.0073, and 0.0044 as shown in Table 6, which are low values for RMSEP and MAPE; thus, the model is suitable to estimate the drug release rate values from MOF materials.

The predicted and experimental values of drug release rate percentage for the training and test sets are shown in Fig. 2. It well proves that the predicted values of drug release rate percentage are fitted on the experimental values.

As can be observed from Table 7, the standard error (SE) for all descriptors are low values, which confirms that the proposed model is appropriate and robust. The probability values (p-values) of the descriptors are very small, confirming that the data could have occurred under the null hypothesis. Other parameters, such as t-test, significance level, and lower and upper bound values for descriptors are presented in Table 7. It can be concluded from Table 7 that all variables in eqn (8) have large effects on the resulting model. The VIF and tolerance for these descriptors are near 1, showing that there is no intercorrelation among the variables.

MOF design and RES calculation are accomplished through the descriptors in eqn (8) and also by considering the "mean effect". Two parameters are involved the "mean effect": (a) the coefficient of descriptors and (b) the nature of descriptors. The value assigned to the nature of descriptors may be positive or negative (Table 1); the coefficient of descriptors can also be positive or negative (the coefficients that appear in eqn (8)). After putting the values of the descriptors in eqn (8), the MOF design can be performed.[104]

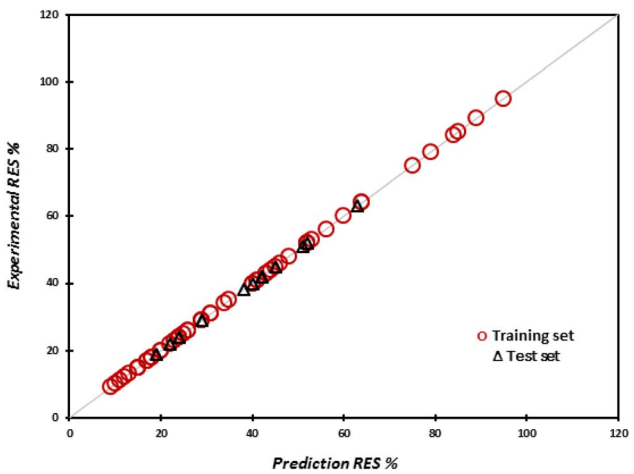

Fig. 2 Predicted values of drug release rate for the training and test sets *versus* the experimental values of drug release rate.

Table 7 Regression coefficients of eqn (8), the standard error (S.E.), *P*-values, *t*-test, and confidence intervals for descriptors

Equation	Des.[a]	Coef.[b]	S.E.[c]	*P*-Value	*t*-Test	Sig.[d]	L.B.[e] (95%)	U.B.[f] (95%)
Eqn (8)	Int.[g]	20.135	0.0021	1.563×10^{-155}	9662.987	<0.0001	20.139	20.130
	n_N	15.157	0.0004	5.7733×10^{-184}	36 759.32	<0.0001	15.158	15.156
	n_O	2.675	0.0001	2.76×10^{-180}	30 922.6	<0.0001	2.675	2.675
	RES^+	−7.301	0.0005	1.4903×10^{-166}	−16219	<0.0001	−7.300	−7.302
	RES^-	14.296	0.0004	9.219×10^{-184}	36 409.89	<0.0001	14.297	14.296

[a] Descriptor. [b] Coefficients. [c] Standard error. [d] Significance level. [e] Lower bound. [f] Upper bound. [g] Intercept.

For further assessment, the cross-validation method was used to make sure overfitting did not occur in modeling.[105] Therefore, leave-one-out (LOO) and y-randomization (yrand) procedures were employed as cross-validation techniques. The values of R_{LOO}^2 and R_{yrand}^2 were obtained at 0.999 and 0.206, respectively. The resulting values confirm the model's accuracy in predicting the release rate percentage (RES%) from MOFs. Also, $R_{yrand}^2 > 0.5$ indicated that there is no chance correlation in the model. Moreover, the Durbin–Watson (DW) statistic of the proposed model was obtained at 2.453, which indicates that there is no autocorrelation in the residuals from the BMLR model. The acceptable range of DW is 1.50–2.50.

4. Conclusion

In this work, a straightforward and robust MLR model has been established, for the first time, to estimate the drug release rate from a set of 67 MOF materials containing different metal SBUs and various organic linkers. The QSPR model was based on four variables, which include the number of nitrogen and oxygen atoms calculated from MOF structures, as well as RES^+ and RES^-, new descriptors that play increaser and decreaser roles. These descriptors were not calculated using software or any complex method, but were computed using a simple and fast procedure. The R^2 value was 0.9999 for both training and test sets. Also, other statistical parameters, including RMSEP, MSE, and MAPE, were satisfactory and confirmed the suitable reliability of eqn (8). The external validation proved that the model is valid for data beyond the dataset used to fit the model. Thus, the present QSPR model enables us to build a straightforward method for predicting drug release rates from MOFs using their structural configuration. As a view towards the future, we are developing QSPR models of MOF-based DDS for other important drugs.

Data and software availability

This QSPR method—applying the number of atoms and adjusted descriptors (computed through chemistry knowledge and tedious work as increaser and decreaser parameters)—is considered proprietary; moreover, it can be used without any complex software and quantum methods. Therefore, this work has unique scientific value, and we share in Table S1 (ESI)† the metal center geometries as a decreaser descriptor, and in Table 4 the ligand fragments as a decreaser descriptor. Finally, the free version of Microsoft Excel 365, with no download needed, was utilized for calculating statistical parameters.

Conflicts of interest

The authors declare that they have no known competition for financial interests or personal relationships that could have influenced the work reported in this paper. The corresponding author states that there is no conflict of interest.

Acknowledgements

The authors gratefully acknowledge from the Iran University of Science and Technology.

References

1 S. Maman and I. P. Witz, *Nat. Rev. Cancer*, 2018, **18**, 359–376.
2 A. C. Garrido-Castro, N. U. Lin and K. Polyak, *Cancer Discovery*, 2019, **9**, 176–198.
3 V. Krishnamoorthy and R. Vilwanathan, *Genomics*, 2020, **112**, 3703–3712.
4 S. Suryavanshi, A. Choudhari, P. Raina and R. Kaul-Ghanekar, *J. Ethnopharmacol.*, 2019, **242**, 112022.
5 A. P. Mishra, B. Salehi, M. Sharifi-Rad, R. Pezzani, F. Kobarfard, J. Sharifi-Rad and M. Nigam, *Mol. Diagn. Ther.*, 2018, **22**, 281–295.
6 A. Yimit, O. Adebali, A. Sancar and Y. Jiang, *Nat. Commun.*, 2019, **10**, 1–11.
7 K. Szyfter, M. Napierala, E. Florek, B. J. Braakhuis, R. P. Takes, J. P. Rodrigo, A. Rinaldo, C. E. Silver and A. Ferlito, *Int. J. Cancer*, 2019, **144**, 2635–2643.
8 D. C. Wolf, S. M. Cohen, A. R. Boobis, V. L. Dellarco, P. A. Fenner-Crisp, A. Moretto, T. P. Pastoor, R. S. Schoeny, J. G. Seed and J. E. Doe, *Regul. Toxicol. Pharmacol.*, 2019, **103**, 86–92.
9 M. Fiore, G. Oliveri Conti, R. Caltabiano, A. Buffone, P. Zuccarello, L. Cormaci, M. A. Cannizzaro and M. Ferrante, *Int. J. Environ. Res.*, 2019, **16**, 1185.
10 P. Rawla and A. Barsouk, *Przegl. Gastroenterol.*, 2019, **14**, 26.
11 B. Singh and S. Mitragotri, *Biotechnol. Adv.*, 2019, **42**, 107339.
12 E. M. Michalak, M. L. Burr, A. J. Bannister and M. A. Dawson, *Nat. Rev. Mol. Cell Biol.*, 2019, **20**, 573–589.

13 R. Oun, Y. E. Moussa and N. J. Wheate, *Dalton Trans.*, 2018, **47**, 6645–6653.
14 G. Spengler, M. Gajdács, M. A. Marć, E. Domínguez-Álvarez and C. Sanmartín, *Molecules*, 2019, **24**, 336.
15 J. Kanduri, L. A. More, A. Godishala and A. Asnani, *Cardiol. Clin.*, 2019, **37**, 399–405.
16 A. Montazerabadi, J. Beik, R. Irajirad, N. Attaran, S. Khaledi, H. Ghaznavi and A. Shakeri-Zadeh, *Artif. Cells, Nanomed., Biotechnol.*, 2019, **47**, 330–340.
17 Q. Zhou, L. Zhang, T. Yang and H. Wu, *Int. J. Nanomed.*, 2018, **13**, 2921.
18 H. Guo, Y. Xia, K. Feng, X. Qu, C. Zhang and F. Wan, *Int. J. Nanomed.*, 2020, **15**, 3235.
19 M. Y. Masoomi, A. Morsali, A. Dhakshinamoorthy and H. Garcia, *Angew. Chem., Int. Ed.*, 2019, **58**, 15188–15205.
20 B. J. Neves, R. C. Braga, C. C. Melo-Filho, J. T. Moreira-Filho, E. N. Muratov and C. H. Andrade, *Front. Pharmacol.*, 2018, **9**, 1275.
21 L. Bouarab-Chibane, V. Forquet, P. Lantéri, Y. Clément, L. Léonard-Akkari, N. Oulahal, P. Degraeve and C. Bordes, *Front. Microbiol.*, 2019, **10**, 829.
22 S. Kwon, H. Bae, J. Jo and S. Yoon, *BMC Bioinf.*, 2019, **20**, 1–12.
23 T. N. Borhani, S. García-Muñoz, C. V. Luciani, A. Galindo and C. S. Adjiman, *Phys. Chem. Chem. Phys.*, 2019, **21**, 13706–13720.
24 T. Gafourian, A. Safari, K. Adibkia, F. Parviz and A. Nokhodchi, *J. Pharm. Sci.*, 2007, **96**, 3334–3351.
25 T. Ghafourian, P. Zandasrar, H. Hamishekar and A. Nokhodchi, *J. Controlled Release*, 2004, **99**, 113–125.
26 T. Ghafourian, M. Barzegar-Jalali, S. Dastmalchi, T. Khavari-Khorasani, N. Hakimiha and A. Nokhodchi, *Int. J. Pharm.*, 2006, **319**, 82–97.
27 I. Tsamardinos, G. S. Fanourgakis, E. Greasidou, E. Klontzas, K. Gkagkas and G. E. Froudakis, *Microporous Mesoporous Mater.*, 2020, **300**, 110160.
28 J. Burner, L. Schwiedrzik, M. Krykunov, J. Luo, P. G. Boyd and T. K. Woo, *J. Phys. Chem. C*, 2020, **124**, 27996.
29 C. Altintas, O. F. Altundal, S. Keskin and R. Yildirim, *J. Chem. Inf. Model.*, 2021, **61**, 5.
30 M. Keshavarz and A. Akbarzadeh, *SAR QSAR Environ. Res.*, 2019, **30**, 347–361.
31 A. Akbarzadeh, M. Nekoeifard, R. Rahmatollah and M. Keshavarz, *SAR QSAR Environ. Res.*, 2020, **31**, 347–371.
32 J. Wang, J. Jin, F. Li, B. Li, J. Liu, J. Jin, C. Wang, Y. Zeng and Y. Wang, *RSC Adv.*, 2015, **5**, 85606–85612.
33 K. Xing, R. Fan, F. Wang, H. Nie, X. Du, S. Gai, P. Wang and Y. Yang, *ACS Appl. Mater. Interfaces*, 2018, **10**, 22746–22756.
34 C. Y. Sun, C. Qin, C. G. Wang, Z. M. Su, S. Wang, X. L. Wang, G. S. Yang, K. Z. Shao, Y. Q. Lan and E. B. Wang, *Adv. Mater.*, 2011, **23**, 5629–5632.
35 B. Yang, M. Shen, J. Liu and F. Ren, *Pharm. Res.*, 2017, **34**, 2440–2450.
36 Y. Zhang and J. Wang, *Inorg. Chim. Acta*, 2018, **477**, 8–14.
37 Y. Cai, Z. Sheng and J. Wang, *Z. Anorg. Allg. Chem.*, 2018, **644**, 877–882.
38 F. Li, C. Gu, H. Li, J. Xu and J. Liu, *J. Inorg. Organomet. Polym. Mater.*, 2017, **27**, 334–341.
39 Q. L. Li, J. P. Wang, W. C. Liu, X. Y. Zhuang, J. Q. Liu, G.-L. Fan, B.-H. Li, W.-N. Lin and J.-H. Man, *Inorg. Chem. Commun.*, 2015, **55**, 8–10.
40 J. S. Qin, D. Y. Du, W. L. Li, J. P. Zhang, S. L. Li, Z. M. Su, X. L. Wang, Q. Xu, K. Z. Shao and Y. Q. Lan, *Chem. Sci.*, 2012, **3**, 2114–2118.
41 W. Zhang, Y. B. Ma, Y. A. Li and H. P. Wang, *J. Iran. Chem. Soc.*, 2019, **16**, 65–71.
42 D. Y. Ma, J. Xie, Z. Zhu, H. Huang, Y. Chen, R. Su and H. Zhu, *Inorg. Chem. Commun.*, 2017, **86**, 128–132.
43 X.-T. Xin and J.-Z. Cheng, *J. Coord. Chem.*, 2018, **71**, 3565–3574.
44 Z. C. Wang, Y. Zhang and Z. Y. Li, *J. Cluster Sci.*, 2018, **29**, 1285–1290.
45 Z. Yan, X. Li, Q. Fan, H. Bai, S. Wu, Z. F. Zhang and L. Pan, *J. Mol. Struct.*, 2020, **1204**, 127477.
46 P. P. Bag, D. Wang, Z. Chen and R. Cao, *Chem. Commun.*, 2016, **52**, 3669–3672.
47 B. Yan, H. Li, W. Jiang and L. Mu, *Aust. J. Chem.*, 2018, **71**, 978–982.
48 Z. Y. Lv, X. R. Zhao and L. Zhao, *J. Iran. Chem. Soc.*, 2019, **16**, 757–763.
49 D. Wang, X. Liu, X. Ye, K. Yuan, X. Xing, Y. Xie, Z. Chen, B. Li, C. Huang and T. Kuang, *Mater. Express*, 2020, **10**, 934–941.
50 S. A. Noorian, N. Hemmatinejad and J. A. Navarro, *Microporous Mesoporous Mater.*, 2020, **302**, 110199.
51 D. C. Zhang and X. Li, *CrystEngComm*, 2017, **19**, 6673–6680.
52 F. Li, B. Li, C. Wang, Y. Zeng, J. Liu, C. Y. Gu, P. Lu and L. Mei, *RSC Adv.*, 2016, **6**, 47959–47965.
53 B. H. Song, X. Ding, C. Li and G. F. An, *Z. Anorg. Allg. Chem.*, 2018, **644**, 472–476.
54 J. Wang, D. Ma, W. Liao, S. Li, M. Huang, H. Liu, Y. Wang, R. Xie and J. Xu, *CrystEngComm*, 2017, **19**, 5244–5250.
55 S. Li, K. Wang, Y. Shi, Y. Cui, B. Chen, B. He, W. Dai, H. Zhang, X. Wang and C. Zhong, *Adv. Funct. Mater.*, 2016, **26**, 2715–2727.
56 F. M. Zhang, H. Dong, X. Zhang, X. J. Sun, M. Liu, D. D. Yang, X. Liu and J. Z. Wei, *ACS Appl. Mater. Interfaces*, 2017, **9**, 27332–27337.
57 F. R. S. Lucena, L. C. de Araújo, M. d. D. Rodrigues, T. G. da Silva, V. R. Pereira, G. C. Militão, D. A. Fontes, P. J. Rolim-Neto, F. F. da Silva and S. C. Nascimento, *Biomed. Pharmacother.*, 2013, **67**, 707–713.
58 J. Q. Liu, J. Wu, Z. B. Jia, H. L. Chen, Q. L. Li, H. Sakiyama, T. Soares, R. Fei, C. Daiguebonne and O. Guillou, *Dalton Trans.*, 2014, **43**, 17265–17273.
59 J. Q. Liu, X. F. Li, C. Y. Gu, J. C. da Silva, A. L. Barros, S. Alves Jr, B. H. Li, F. Ren, S. R. Batten and T. A. Soares, *Dalton Trans.*, 2015, **44**, 19370–19382.
60 C. Gu, F. Li, B. Li, J. Xu, S. Yang, M. Luo, J. Liu and G. Liu, *Inorg. Chem. Commun.*, 2016, **73**, 26–29.
61 W. Liu, Y. Zhong, X. Wang, C. Zhuang, J. Chen, D. Liu, W. Xiao, Y. Pan, J. Huang and J. Liu, *Inorg. Chem. Commun.*, 2020, **111**, 107675.

62 J. Wu, J. W. Xu, W. C. Liu, S. Z. Yang, M. M. Luo, Y. Y. Han, J. Q. Liu and S. R. Batten, *Inorg. Chem. Commun.*, 2016, **71**, 32–34.
63 E. H. Zhou, R. Wang, J. Wu, S. W. Qiu, J. Q. Liu, H. R. Zhong, H. D. Zeng, J. W. Xu and J. C. Jin, *Bull. Chem. Soc. Ethiop.*, 2017, **31**, 457–463.
64 R. Li, S. Liu, Q. Tang, T. Wang, Y. Xie and R. Zhai, *Z. Anorg. Allg. Chem.*, 2018, **644**, 317–321.
65 L. Chen, H. Yu, Y. Li, X. Zhang and Y. Du, *Struct. Chem.*, 2018, **29**, 1885–1891.
66 Y. Guo, B. Yan, Y. Cheng and L. Mu, *J. Coord. Chem.*, 2019, **72**, 262–271.
67 L. L. Sun, Y. H. Li and H. Shi, *J. Cluster Sci.*, 2019, **30**, 251–258.
68 M. Ren, H. Li, H. Liu, L. Wang, H. Xiang, X. Zhang and B. Yu, *Aust. J. Chem.*, 2018, **72**, 233–239.
69 H. T. Li, S. J. Song, X. R. Pei and D. B. Lu, *Z. Anorg. Allg. Chem.*, 2019, **645**, 801–809.
70 Q. Q. Wang, Z. P. Yang, Z. T. Cui, X. H. Wang and Y. Lin, *J. Coord. Chem.*, 2020, **73**, 1436–1449.
71 D. Li, L. F. Li, Z. F. Zhang, D. Xue, L. Pan and Y. Liu, *J. Coord. Chem.*, 2020, **73**, 266–281.
72 Z. Hu, C. Qiao, Z. Xia, F. Li, J. Han, Q. Wei, Q. Yang, G. Xie, S. Chen and S. Gao, *ACS Appl. Mater. Interfaces*, 2020, **12**, 14914–14923.
73 F. Wang, J. Wang, S. Yang, C. Gu, X. Wu, J. Liu, H. Sakiyama, J. Xu, M. Luo and W. Liu, *Russ. J. Coord. Chem.*, 2017, **43**, 133–137.
74 X. E. Feng and T. T. Zhu, *Inorg. Nano-Met. Chem.*, 2020, **50**, 1302–1307.
75 Q. Zhang, J. Zhao, Y. Li, X. Wu, L. Ma and Z. Ding, *Russ. J. Coord. Chem.*, 2020, **46**, 584–591.
76 B. E. Souza and J.-C. Tan, *CrystEngComm*, 2020, **22**, 4526–4530.
77 S. Tai, W. Zhang, J. Zhang, G. Luo, Y. Jia, M. Deng and Y. Ling, *Microporous Mesoporous Mater.*, 2016, **220**, 148–154.
78 B. Miri, N. Motakef-Kazemi, S. A. Shojaosadati and A. Morsali, *Iran. J. Pharm. Res.*, 2018, **17**, 1164.
79 L. Li, S. Han, C. Yang, L. Liu, S. Zhao, X. Wang, B. Liu, H. Pan and Y. Liu, *Nanotechnology*, 2020, **31**, 325602.
80 X. Gao, Y. Wang, G. Ji, R. Cui and Z. Liu, *CrystEngComm*, 2018, **20**, 1087–1093.
81 L. L. Tan, H. Li, Y. Zhou, Y. Zhang, X. Feng, B. Wang and Y. W. Yang, *Small*, 2015, **11**, 3807–3813.
82 X. Du, R. Fan, L. Qiang, K. Xing, H. Ye, X. Ran, Y. Song, P. Wang and Y. Yang, *ACS Appl. Mater. Interfaces*, 2017, **9**, 28939–28948.
83 Z. Jiang, B. Yuan, N. Qiu, Y. Wang, L. Sun, Z. Wei, Y. Li, J. Zheng, Y. Jin and Y. Li, *Nano-Micro Lett.*, 2019, **11**, 1–17.
84 W. Liu, Y. Pan, Y. Zhong, B. Li, Q. Ding, H. Xu, Y. Qiu, F. Ren, B. Li and M. Muddassir, *Chem. Eng. J.*, 2021, **412**, 127899.
85 C. Liu, X. Xu, J. Zhou, J. Yan, D. Wang and H. Zhang, *BMC Materials*, 2020, **2**, 1–11.
86 C. Zou, Z. Wang, X. Ren, R. Li, S. Zhang and B. Sheng, *Inorg. Chem. Commun.*, 2018, **91**, 91–94.
87 Z. Luo, R. Wang, C. Gu, F. Li, Y. Han, B. Li and J. Liu, *Inorg. Chem. Commun.*, 2017, **76**, 91–94.
88 M. Rezaei, A. Abbasi, R. Dinarvand, M. Jeddi-Tehrani and J. Janczak, *ACS Appl. Mater. Interfaces*, 2018, **10**, 17594–17604.
89 C. Y. Sun, C. Qin, X. L. Wang, G. S. Yang, K. Z. Shao, Y. Q. Lan, Z. M. Su, P. Huang, C. G. Wang and E. B. Wang, *Dalton Trans.*, 2012, **41**, 6906–6909.
90 X. Xiao, S. Liang, Y. Zhao, D. Huang, B. Xing, Z. Cheng and J. Lin, *Nanoscale*, 2020, **12**, 3846–3854.
91 H. N. Wang, G. S. Yang, X. L. Wang and Z. M. Su, *Dalton Trans.*, 2013, **42**, 6294–6297.
92 F. J. Liu and B. M. Xu, *Z. Anorg. Allg. Chem.*, 2018, **644**, 821–826.
93 H. Dong, G. X. Yang, X. Zhang, X. B. Meng, J. L. Sheng, X. J. Sun, Y. J. Feng and F. M. Zhang, *Chem.–Eur. J.*, 2018, **24**, 17148–17154.
94 X. G. Wang, L. Xu, M. J. Li and X. Z. Zhang, *Angew. Chem., Int. Ed.*, 2020, **59**, 18078–18086.
95 A. Ma, Z. Luo, C. Gu, B. Li and J. Liu, *Inorg. Chem. Commun.*, 2017, **77**, 68–71.
96 B. H. Song, X. Ding, Z. F. Zhang and G. F. An, *J. Iran. Chem. Soc.*, 2019, **16**, 333–340.
97 L. C. Zhao, M. Tang, Q. H. Zhang, Z. Y. Hu, H. W. Gao, X. Y. Liao, G. Wang and J. Leng, *J. Chem.*, 2018, **2018**, 1–7.
98 D. Wei, Y. Xin, Y. Rong, Y. Li, C. Zhang, Q. Chen, S. Qin, W. Wang and Y. Hao, *J. Inorg. Organomet. Polym. Mater.*, 2020, **30**, 1121–1131.
99 H. N. Wang, X. Meng, X. L. Wang, G. S. Yang and Z. M. Su, *Dalton Trans.*, 2012, **41**, 2231–2233.
100 Y. Liu, L. W. Shen and M. X. Song, *Main Group Chem.*, 2019, **18**, 427–436.
101 Y. Li, X. Li, Q. Guan, C. Zhang, T. Xu, Y. Dong, X. Bai and W. Zhang, *Int. J. Nanomed.*, 2017, **12**, 1465.
102 X. Gao, M. Zhai, W. Guan, J. Liu, Z. Liu and A. Damirin, *ACS Appl. Mater. Interfaces*, 2017, **9**, 3455–3462.
103 R. Krishnamurthy and W. B. Schaap, *J. Chem. Educ.*, 1969, **46**, 799.
104 M. Moharramnejad, L. Tayebi, A. R. Akbarzadeh and A. Maleki, *Microporous Mesoporous Mater.*, 2022, **336**, 111815.
105 X. Ying, *J. Phys.: Conf. Ser.*, 2019, **1168**, 022022.